



Soft Matter

Nonlinear microrheology of active Brownian suspensions

Journal:	<i>Soft Matter</i>
Manuscript ID	SM-ART-08-2019-001713.R1
Article Type:	Paper
Date Submitted by the Author:	20-Nov-2019
Complete List of Authors:	Burkholder, Eric; Stanford University, Physics Brady, John; California Institute of Technology, Department of Chemical Engineering

SCHOLARONE™
Manuscripts

Cite this: DOI: 10.1039/xxxxxxxxxx

Nonlinear microrheology of active Brownian suspensions

Eric W. Burkholder,^{a†} John F. Brady,^{a,b*}Received Date
Accepted Date

DOI: 10.1039/xxxxxxxxxx

www.rsc.org/journalname

The rheological properties of active suspensions are studied via microrheology: tracking the motion of a colloidal probe particle in order to measure the viscoelastic response of the embedding material. The passive probe particle with size R is pulled through the suspension by an external force F^{ext} , which causes it to translate at some speed U^{probe} . The bath is comprised of a Newtonian solvent with viscosity η_s and a dilute dispersion of active Brownian particles (ABPs) with size a , characteristic swim speed U_0 , and a reorientation time τ_R . The motion of the probe distorts the suspension microstructure, so the bath exerts a reactive force on the probe. In a passive suspension, the degree of distortion is governed by the Péclet number, $Pe = F^{ext}/(k_B T/a)$, the ratio of the external force to the thermodynamic restoring force of the suspension. In active suspensions, however, the relevant parameter is $L^{adv}/\ell = U^{probe} \tau_R / U_0 \tau_R \sim F^{ext} / F^{swim}$, where $F^{swim} = \zeta U_0$ is the swim force that propels the ABPs (ζ is the Stokes drag on a swimmer). When the external forces are weak, $L^{adv} \ll \ell$, the autonomous motion of the bath particles leads to “swim-thinning,” though the effective suspension viscosity is always greater than η_s . When advection dominates, $L^{adv} \gg \ell$, we recover the familiar behavior of the microrheology of passive suspensions. The non-Newtonian behavior for intermediate values of L^{adv}/ℓ is determined by $\ell/R_c = U_0 \tau_R / (R + a)$ —the ratio of the swimmer’s run length ℓ to the geometric length scale associated with interparticle interactions R_c . The results in this manuscript are approximate as they are based on numerical solutions to mean-field equations that describe the motion of the active bath particles.

1 Introduction

The focus of many theoretical and experimental investigations in soft-matter physics has turned to the dynamic behavior of colloidal suspensions of self-propelled particles, an example of active matter. These systems pose an interesting challenge as their constituents are able to generate their own internal stresses and drive a suspension out of equilibrium without the influence of external forces^{1,2}. These inherently far-from-equilibrium materials do not obey typical thermodynamic relationships—e.g. the fluctuation-dissipation theorem (FDT)^{3,4}—and exhibit fascinating behaviors such as spontaneous collective motion^{5–11}.

Macroscopic measurements of the shear-viscosity of active suspensions have shown the potential for highly active suspensions of tail-actuated, anisotropic swimmers under weak shear to reach a superfluid-like state in which the total shear stress measured

by bulk rheometry is zero—or even negative^{12,13}. Theoretical models suggest that the origin of this “superfluid” behavior is the active hydrodynamic stress exerted by the swimmer on the surrounding fluid; thus, this effect would only be observed in suspensions of anisotropic particles. The hydrodynamic stress of an extensile swimmer (“pusher”) or contractile swimmer (“puller”) will either decrease or increase the apparent viscosity, respectively¹⁴. These effects are hydrodynamic in origin, and reflect the interaction of the swimmer with the fluid under shear, not the interaction between swimmers in suspension.

Reductions in the zero-shear viscosity of suspensions of anisotropic active particles thus give rise to non-Newtonian suspension rheology, even at the single-particle level. The shear viscosity of the suspension depends on the ratio of the shear-rate $\dot{\gamma}$ to the rotary diffusion rate τ_R^{-1} of the swimmers, which defines a Péclet number $Pe_{\dot{\gamma}} = \dot{\gamma} \tau_R$. When $Pe_{\dot{\gamma}} \ll 1$ swimming is dominant and the active particles may greatly reduce the zero-shear Newtonian plateau^{12–14}. When $Pe_{\dot{\gamma}} \gg 1$, the fluid flow is able to overwhelm the active random motion of the swimmers and align them with the rate-of-strain field—this gives Brenner’s familiar correction to the shear viscosity for a single particle¹⁵. This transition is non-monotonic in $Pe_{\dot{\gamma}}$ —thus the suspension goes from being

^a Division of Chemistry and Chemical Engineering, California Institute of Technology, Pasadena, CA 91125 USA.

^b Division of Engineering and Applied Science, California Institute of Technology, Pasadena, CA 91125 USA

* Email: jfbrady@caltech.edu

† Current address: Department of Physics, Stanford University, Stanford, CA 94305 USA.

Newtonian in the absence of activity (at the single-particle level) to non-monotonically shear thickening¹⁴. In passive colloidal suspensions, shear-thickening can only arise at the pair-level, and is usually attributed to lubrication interactions or frictional contact forces between particles^{16,17}.

Though the bulk rheological behavior of active fluids is interesting, the local (microscopic) behavior is often of greater relevance in suspensions of active particles. Microrheology—which measures the local viscous response via the drag on a colloidal probe particle—is an ideal framework for analyzing the suspension mechanics of active systems because it does not require large sample volumes, which may be prohibitively expensive or experimentally unrealizable for active biological materials, and it can probe micro-scale heterogeneity in the material structure¹⁸. For example, the interior of a cell may be modeled as a concentrated colloidal dispersion wherein many of the constituents are self-propelled (i.e. motor proteins). Understanding how the activity of biocolloids affects the micro-mechanics of such systems promises to give greater understanding of fundamental cellular processes, such as cellular reproduction where cytoskeletal filaments undergo directed motion by motor proteins in preparation for mitosis. (How would the active motion of other cellular components affect the force required to move these filaments?) Enhanced understanding of these biological processes may enable more effective drug delivery and gene therapy at the cellular level^{19,20}.

Macrorheology and microrheology measure fundamentally different quantities: macrorheology measures the material response at length scales on the order of the gap distance between two surfaces (usually in the range of a few millimeters), whereas microrheology measures the material response on the order of the probe size (a few microns). The two methods measure distinct viscoelastic properties that may not quantitatively agree with one another. Qualitatively, however, the two methods have shown remarkable agreement²¹. Indeed, even quantitative agreement between the Einstein viscosity correction and microviscosity has been found in the limit of a large probe particle moving in a suspension of point bath particles, as would be expected²².

Relatively little attention has been given to the microrheology problem in active media^{3,4,13,23,24}. The linear microrheology problem has been studied in the context of the fluctuation-dissipation relation in active materials^{3,4}, and in studies of active nematics^{23,25}. In contrast to microrheology of passive suspensions, Foffano et al. find stark qualitative differences between the microrheology and macrorheology of an active nematic²⁵; a negative microviscosity was found for contractile suspensions, whereas negative shear-viscosities are usually associated with extensile suspensions²³. To-date, no studies have investigated the viscoelastic response of active suspensions when subjected to non-linear microscopic deformations—when the external force is comparable to or much larger than both the thermal energy $k_B T$ and the activity of the swimmers.

In this paper, we extend our previous investigation of the linear microrheology of an active Brownian suspension to the non-linear regime. In that study we calculated the average speed of a probe particle of size R moving slowly through a suspension

of active Brownian particles (ABPs) with swim speed U_0 , size a and reorientation time τ_R . The relative thermal Stokes-Einstein-Sutherland diffusivity of the probe-swimmer pair was D^{rel} and the center-to-center separation distance of the probe-swimmer pair upon contact was $R_c = R + a$. In our previous study we implicitly assumed that the distance moved by the probe during a time τ_R , $L^{adv} = U^{probe} \tau_R$ (where U^{probe} is the probe speed) was small compared to the run length of the swimmers $\ell = U_0 \tau_R$. The run length of the swimmers was varied with respect to the length scale of Brownian motion $\delta = \sqrt{D^{rel} \tau_R}$ and the size of the particles R_c . In this paper, we relax the constraint on probe speed and allow L^{adv}/ℓ to become $\gtrsim O(1)$. Based on previous work^{4,26} we offer some predictions of the microrheological behavior in the non-linear regime.

When $L^{adv} \ll \ell$ the swimmers travel a much greater distance ℓ between reorientations than does the probe. The swimmers are thus able to bombard the probe equally well from all directions and keep up with it as it moves. The microviscosity is determined only by the strength of activity relative to thermal fluctuations and the particle sizes, ℓ/R_c and ℓ/δ , and is the same as we found previously⁴. Active suspensions exhibit a weak-force Newtonian plateau that is the same as that found in passive suspensions when $\ell \gg R_c$ or $\ell \ll R_c$, but lower when the run length is comparable to the contact length $\ell \sim R_c$ —the suspension exhibits swim-thinning that is nonmonotonic in ℓ/R_c and similar for different values of ℓ/δ . In the opposite limit, $L^{adv}/\ell \gg 1$, the probe is moving much farther between swimmers' reorientations than they are. This means that swimmers behind the probe will not be able to fill in the wake left by the probe. Similarly, the swimmers that accumulate in the advective-diffusive boundary layer on the front of the probe are not able to escape and swim out of the probe's way before they reorient. They remain trapped in the boundary layer and accumulate just as if they were passive Brownian particles (top row of Fig. 8). Thus, an active suspension will exhibit the same large-force plateau as found in passive suspensions regardless of ℓ/R_c and ℓ/δ .

When $L^{adv} \sim \ell$, the swimmers and the probe move a comparable distance between reorientations of the active particles. A cartoon of the physical behavior for $L^{adv} \sim \ell$ at various ℓ/R_c may be found in Fig. 1. In what we call the continuum limit $\ell/R_c \ll 1$ the swimmers' motion is effectively Brownian on the length scale of probe motion. Neither the swimmers nor the probe move a substantial distance compared to R_c during the time τ_R . The swimmers keep pace with the probe, but are not able to move out of the probe's path in front or get into the wake behind. Thus, the activity has little effect on the non-Newtonian behavior, and the suspension force-thins from the low-force Newtonian plateau to the high force Newtonian plateau, just like a suspension of passive particles²⁷.

Next, consider the case when $\ell/R_c \gg 1$ (Fig. 1, bottom panel). Particles will accumulate at the front of the probe due to advection as they do in passive suspensions, but some of the particles will be able to escape the advective-diffusive boundary layer and swim out of the probe's path. Conversely, some of the particles behind the probe will be able to fill in the wake, or even collide with the probe from behind. Both of these behaviors tend to

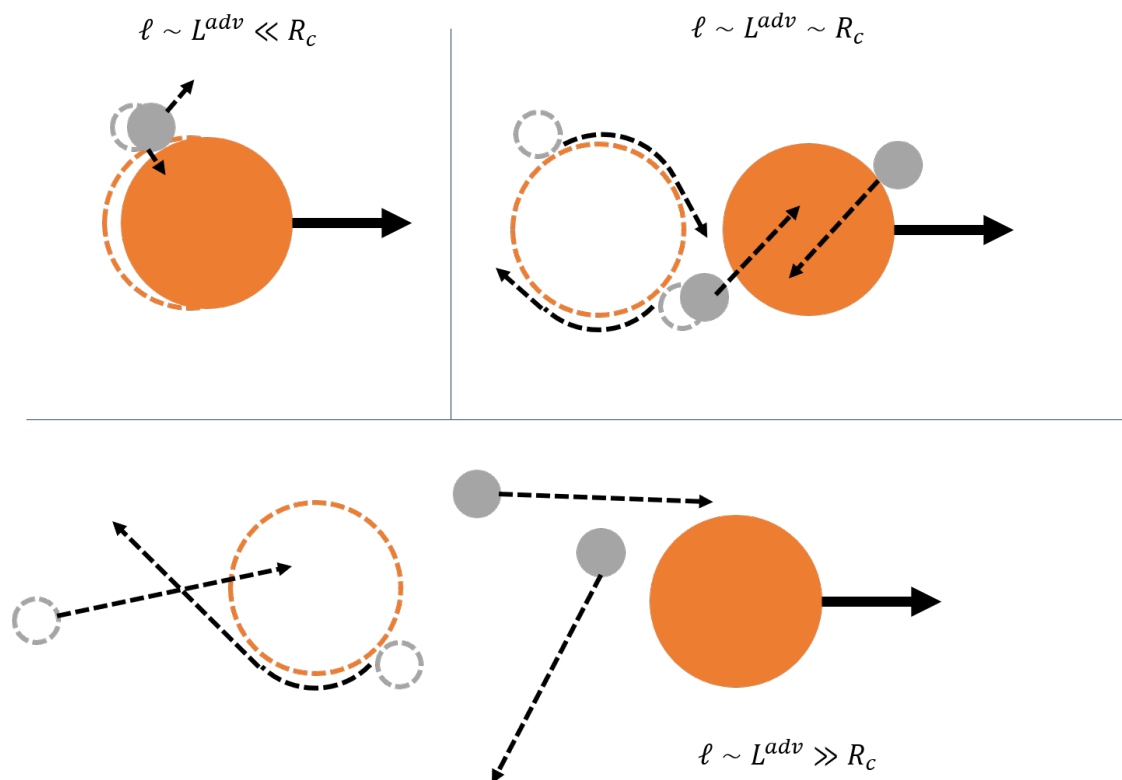


Fig. 1 Sketch of swimmer trajectories for various $\ell/R_c = U_0 \tau_R/R_c$ and $L^{adv} = U^{probe} \tau_R \sim \ell$. The swimmer's reorientation time and swim speed are τ_R and U_0 , respectively, and the probe speed is U^{probe} ; R_c is the center-to-center separation distance of a probe-swimmer pair at contact. In each panel, the dashed circles represent the probe (orange) and bath (grey) particle positions at a time τ_R before the solid circles. Top Left: when $\ell \ll R_c$ the swimmer reorients quickly after colliding with the probe, behaving no differently than a Brownian particle. The microrheology is thus similar to passive suspensions (Fig. 7, left) Top right: when $\ell \sim R_c$ swimmers that slide to the front of the probe upon collision are more likely to reorient and push against the probe, while swimmers that slide to the rear of the probe will be left behind as the probe continues moving forward. This is the physical mechanism for force-thickening (see Fig. 7, center). Bottom panel: when $\ell \sim L^{adv} \gg R_c$, swimmers behind the probe are unable to keep up with it, and swimmers that collide with the probe and slide to the back are similarly unable to keep up with it. As a result, the suspension microviscosity is no different than that in a passive suspension (Fig. 7, right).

decrease the apparent viscosity of the suspension, and thus the force-thinning behavior seen in passive suspensions is retained in this limit. For $\ell \sim R_c$ (Fig. 1, top right), swimmers near the probe remain within striking distance of the probe surface after reorientations when $L^{adv} \ll \ell$. On average, more swimmers ended up pushing the probe forward than pushing against the probe. When the probe speed increases, the swimmers behind the probe now have more difficulty pushing the probe along because it is travelling approximately the same distance as they are in a time τ_R . The opposite is true for the swimmers pushing against the probe out front. Thus, the suspension will actually force-thicken in this regime. This is notable, as force-thickening in passive suspensions arises from hydrodynamic lubrication interactions, which we have neglected here. This force-thickening is non-monotonic.

In the next section we write down the Smoluchowski equation that describes the dynamics of a passive Brownian probe particle moving through a suspension of active Brownian bath particles (ABPs). We then review the results of Yan & Brady²⁶ and Burkholder & Brady⁴ for the case of a stationary and slowly-moving probe, respectively. Finally, we compute the nonlinear microviscosity for arbitrary values of ℓ/δ , ℓ/R_c , and L^{adv}/ℓ by numerically solving orientation-averaged moments of the Smolu-

chowski equation²⁸. These calculations confirm the above physical predictions of the force-dependent microrheology of active suspensions.

2 Theoretical framework

We consider a dispersion of $N - 1$ swimmers and one passive probe particle of size R with thermal Stokes-Einstein-Sutherland (SES) diffusivity D_P in a Newtonian solvent with viscosity η_s . The swimmers are modeled as active Brownian particles (ABPs) with size a , (constant) swim speed U_0 , thermal SES diffusivity D_T , and a characteristic reorientation time τ_R . The probe moves at speed U^{probe} due to an applied external force F^{ext} ; either the force or probe speed may be fixed. The dynamics of this suspension are described by a Smoluchowski equation in position and orientation space:

$$\frac{\partial P_N}{\partial t} + \sum_{i=1}^N \nabla_{\mathbf{x}_i} \cdot \mathbf{j}_i^T + \sum_{i=1}^N \nabla_{\mathbf{R}_i} \cdot \mathbf{j}_i^R = 0, \quad (1)$$

which is simply a conservation statement for $P_N(\{\mathbf{x}_i\}, \{\mathbf{q}_i\}; t)$, the time-dependent N -particle probability distribution of the suspension that depends on the positions (\mathbf{x}_i) and orientations (\mathbf{q}_i) of each particle. The rotational operator $\nabla_{\mathbf{R}_i}$ is given by $\mathbf{q}_i \times \nabla_{\mathbf{q}_i}$ for

an axisymmetric particle.

When the suspension is sufficiently dilute ($\phi = 4\pi n^\infty a^3/3 \ll 1$ in three dimensions or $\phi_A = 4\pi a^2 n_A^\infty \ll 1$ in two-dimensions, where n^∞ is the constant volumetric number density of swimmers and n_A^∞ is a constant areal number density of swimmers for $d = 2$) only the pair-wise interactions between the probe and a single swimmer matter. Thus, one can write a Smoluchowski equation for the pair-level probability distribution, $P_2(\mathbf{x}_P, \mathbf{x}_S, \mathbf{q}_P, \mathbf{q}_S; t)$, where the position and orientation of both the probe ($\mathbf{x}_P, \mathbf{q}_P$) and swimmer ($\mathbf{x}_S, \mathbf{q}_S$) are in the laboratory frame. Fluctuations in the probe's position do not affect its average speed due to translational invariance^{29,30} and the orientation of the probe is irrelevant because it is a passive particle. Thus we can average over the phase space of the probe and write the Smoluchowski equation in a relative coordinate frame

$$\frac{\partial P_{1/1}(\mathbf{r}, \mathbf{q}; t)}{\partial t} + \nabla_r \cdot (\mathbf{j}_s^T - \mathbf{j}_p^T) + \nabla_q \cdot \mathbf{j}_s^R = 0, \quad (2)$$

where $P_2(\mathbf{x}_P, \mathbf{x}_S, \mathbf{q}_P, \mathbf{q}_S; t) = P_{1/1}(\mathbf{r}, \mathbf{q}; t)P_1(\mathbf{z}, \mathbf{q}_P; t)$ and we have defined $\mathbf{z} = \mathbf{x}_P$, $\mathbf{r} = \mathbf{x}_S - \mathbf{x}_P$, and $\mathbf{q} = \mathbf{q}_S$. \mathbf{j}_p^T is the translational flux of the probe, and \mathbf{j}_s^T and \mathbf{j}_s^R are the translational and rotational fluxes of the swimmer, respectively. The probability distribution for the probe particle P_1 is not explicitly needed to compute the average probe velocity or diffusivity²⁹. In the absence of hydrodynamic interactions (which we neglect in this study), the translational and rotational flux of the swimmer relative to the probe, respectively, are:

$$\mathbf{j}^T \equiv \mathbf{j}_s^T - \mathbf{j}_p^T = (U_0 \mathbf{q} - \mathbf{U}^{probe})P_{1/1} - D^{rel} \nabla_r P_{1/1}, \quad (3)$$

$$\mathbf{j}_s^R = -\frac{1}{\tau_R} \nabla_q P_{1/1}, \quad (4)$$

where $D^{rel} = D_P + D_T$ for a fixed external force and $D^{rel} = D_T$ when the velocity of the probe is fixed. The probe and swimmer interact via excluded volume interactions and thus the particles may not pass through one another upon a collision: $\mathbf{n} \cdot \mathbf{j}^T = 0$, at $|\mathbf{r}| = R_c \equiv R + a$, where \mathbf{n} is the outward pointing unit normal of the probe.

We solve the Smoluchowski equation using the familiar method popularized by Saintillan and Shelley²⁸ and expand the pair-distribution function in terms of orthogonal tensor harmonics in \mathbf{q} :

$$P_{1/1}(\mathbf{r}, \mathbf{q}; t) = \frac{1}{4\pi} \left(n(\mathbf{r}; t) + \mathbf{q} \cdot \mathbf{m}(\mathbf{r}; t) + (\mathbf{q}\mathbf{q} - \mathbf{I}/d) : \mathbf{Q}(\mathbf{r}; t) + (\mathbf{q}\mathbf{q}\mathbf{q} - \boldsymbol{\alpha} \cdot \mathbf{q}/(d+2)) \odot \mathbf{B} + \dots \right), \quad (5)$$

where d is the spatial dimension and $\boldsymbol{\alpha}$ is the fourth-order isotropic tensor. The operation $:$ is the double dot product and \odot is the triple dot product. The zeroth moment, n is the concentration field, \mathbf{m} is the polar order, \mathbf{Q} is the nematic order, and so on^{28,31}. We make the closure $\mathbf{B} = 0$, or $\langle \mathbf{q}\mathbf{q}\mathbf{q} \rangle = \boldsymbol{\alpha} \cdot \langle \mathbf{q} \rangle / (d+2)$. Note that the third moment $\langle \mathbf{q}\mathbf{q}\mathbf{q} \rangle$ is not zero; it's "traceless" part \mathbf{B} , however, is.

Applying the moments-averaging procedure to the governing

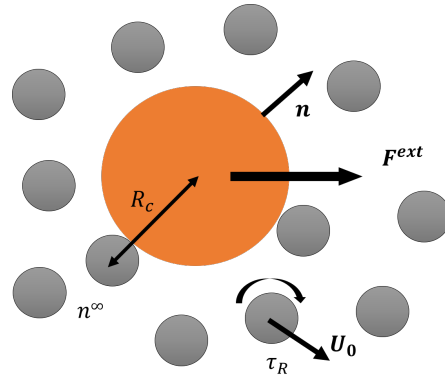


Fig. 2 Schematic of the model system: a Brownian probe particle of size R immersed in a suspension of active Brownian particles (ABPs) with size a at number density n^∞ —the center-to-center separation distance upon a collision is denoted by $R_c = R + a$. The ABPs swim in a direction \mathbf{q} at speed U_0 ; \mathbf{q} changes randomly on a time scale characterized by τ_R . The probe translates under the action of some external force $\mathbf{F}^{ext} = \langle \zeta \rangle \mathbf{U}^{probe}$, which may be constant or specified such that the resulting probe velocity \mathbf{U}^{probe} is constant. The force and velocity are related by the effective drag coefficient (ζ).

equation and boundary conditions for $P_{1/1}$ yields a system of coupled PDEs governing the steady microstructure:

$$\nabla_r \cdot [U_0 \mathbf{m} - D^{rel} \nabla_n - \mathbf{U}^{probe} n] = 0 \quad (6)$$

$$\nabla_r \cdot [U_0 (\mathbf{I}n/d + \mathbf{Q}) - D^{rel} \nabla \mathbf{m} - \mathbf{U}^{probe} \mathbf{m}] + (d-1)D_R \mathbf{m} = 0, \quad (7)$$

$$\nabla_r \cdot [U_0 (\boldsymbol{\alpha} \cdot \mathbf{m}/(d+2) - \mathbf{I}m/d) - D^{rel} \nabla \mathbf{Q} - \mathbf{U}^{probe} \mathbf{Q}] + 2dD_R \mathbf{Q} = 0. \quad (8)$$

At the probe surface there can be no translational flux (i.e. the particles are hard-spheres), and far from the probe the suspension can exhibit no order:

$$\mathbf{n} \cdot \langle \mathbf{j}^T \rangle_q = \mathbf{n} \cdot \langle \mathbf{q}\mathbf{j}^T \rangle_q = \mathbf{n} \cdot \langle (\mathbf{q}\mathbf{q} - \mathbf{I}/d) \mathbf{j}^T \rangle_q = 0, \quad (9)$$

$$\text{at } r = R_c$$

$$n \sim n^\infty, \mathbf{m} \sim \mathbf{0}, \mathbf{Q} \sim \mathbf{0}, \quad r \rightarrow \infty. \quad (10)$$

In the absence of probe motion $P_{1/1}$ is isotropic, so there will be no net force on the probe. Thus, we write the concentration, polar order, and nematic order as the sum of the fields for a stationary probe, plus a perturbation due to the external force: $n = n_0 + n'$, $\mathbf{m} = \mathbf{m}_0 + \mathbf{m}'$, $\mathbf{Q} = \mathbf{Q}_0 + \mathbf{Q}'$. The non-dimensionalized, coupled PDEs for the disturbance fields are:

$$\nabla_r \cdot [(\ell/\delta)^2 (R_c/\ell) \mathbf{m}' - \nabla_r n' - Pe \hat{\mathbf{u}} n'] = Pe \nabla_r \cdot (\hat{\mathbf{u}} n_0), \quad (11)$$

$$\nabla_r \cdot [(\ell/\delta)^2 (R_c/\ell) (\mathbf{I}n'/d + \mathbf{Q}') - \nabla_r \mathbf{m}' - Pe \hat{\mathbf{u}} \mathbf{m}'] \quad (12)$$

$$+ (d-1)(\ell/\delta)^2 (R_c/\ell)^2 \mathbf{m}' = Pe \nabla_r \cdot (\hat{\mathbf{u}} \mathbf{m}_0),$$

$$\begin{aligned} \nabla_r \cdot [(\ell/\delta)^2 (R_c/\ell)(\boldsymbol{\alpha} \cdot \mathbf{m}'/(d+2) - \mathbf{I}\mathbf{m}'/d) - \nabla \mathbf{Q}' - Pe\hat{\mathbf{u}}\mathbf{Q}'] \\ + 2d(\ell/\delta)^2 (R_c/\ell)^2 \mathbf{Q}' = Pe\nabla_r \cdot (\hat{\mathbf{u}}\mathbf{Q}_0), \end{aligned} \quad (13)$$

where $\hat{\mathbf{u}}$ is the unit vector in the direction of probe motion. The scaled governing equations reveal three dimensionless groups. The first is an external Péclet number $Pe = U^{probe} R_c / D^{rel} = F^{ext} / (k_B T / a) = L^{adv} R_c / \delta^2$, where $L^{adv} = U^{probe} \tau_R$ is the distance the probe moves in τ_R and $\delta = \sqrt{D^{rel} \tau_R}$ is the length scale of the thermal fluctuations of the probe and swimmer. This Péclet number reflects the balance between advection and diffusion, which can be expressed in terms of the ratio of the probe speed or advection length to the relevant thermal diffusion length and velocity scales, or in terms of the ratio of the external force to the thermal force. There are two parameters describing the activity of the suspension: (1) a parameter relating the length scale of swimming to the length scale of Brownian fluctuations $\ell/\delta = U_0 \tau_R / \sqrt{D^{rel} \tau_R}$, and (2) a parameter $\ell/R_c = U_0 \tau_R / (R + a)$ that compares the run length of the swimmers to the geometric size of the probe-swimmer pair. We will denote the components of polar order and particle flux in the direction of motion as $m'_{\parallel} = \hat{\mathbf{u}} \cdot \mathbf{m}'$ and $j'_{n,\parallel} = (\ell/\delta)^2 (R_c/\ell) m'_{\parallel} - \hat{\mathbf{u}} \cdot \nabla n' - Pen$, respectively. All fields have been scaled by n^∞ such that the microstructure is unity far from the probe.

The fundamental physical problems in microrheology are to compute: (1) the average velocity of a particle as it is dragged through a suspension by an external force \mathbf{F}^{ext} , or (2) the average force required to make a particle translate through the suspension with velocity \mathbf{U}^{probe} . The former mode is referred to as fixed-force microrheology and the latter is the fixed-velocity mode; in an experimental system the true mode of probing may lie somewhere in between (say, if the probe is being moved by an optical trap of finite potential depth). The differences are discussed in depth in previous works on microrheology in passive systems, but in the absence of hydrodynamic interactions, the two modes differ only by a geometric factor^{27,32}.

The average velocity of the probe as it moves through the suspension is

$$\langle \mathbf{U}^{probe} \rangle = \mathbf{U}^{Stokes} - \frac{1}{\zeta_P} k_B T \int \nabla_r n(\mathbf{r}; t) d\mathbf{r} \quad (14)$$

in the absence of any hydrodynamic interactions or long-ranged interparticle forces^{21,27,33}. The probe's Stokes drag coefficient is $\zeta_P = 6\pi\eta_s R$ and its velocity in a Newtonian solvent is \mathbf{U}^{Stokes} . In the linear-response regime the velocity reduction due to collisions with the bath particles is linear in the applied external force: $\langle \mathbf{U}^{probe} \rangle \sim \mathbf{F}^{ext} \langle \mu \rangle$, where $\langle \mu \rangle$ is the probe mobility; for the fixed-velocity mode $\langle \mathbf{F}^{ext} \rangle \sim \langle \zeta \rangle \mathbf{U}^{probe}$. We define an effective drag coefficient $\langle \zeta \rangle = 6\pi \langle \eta \rangle R$, where $\langle \eta \rangle$ is the microviscosity of the suspension²⁷. In the absence of hydrodynamic interactions, $\langle \mu \rangle = 1/\langle \zeta \rangle$, but this is not true in general.

The effects of interparticle interactions (given by the integral in Eqn. 14) may be characterized by the intrinsic microviscosity $\eta^{micro} = (\langle \zeta \rangle - \zeta_P) / \zeta_P \phi^{ex}$, where $\phi^{ex} = 2\pi a R_c^2 n^\infty / 3$ is the excluded volume fraction. (In 2d this is replaced by the excluded area fraction $\phi_A^{ex} = 2\pi a R_c n_A^\infty$, where n_A^∞ is the areal number den-

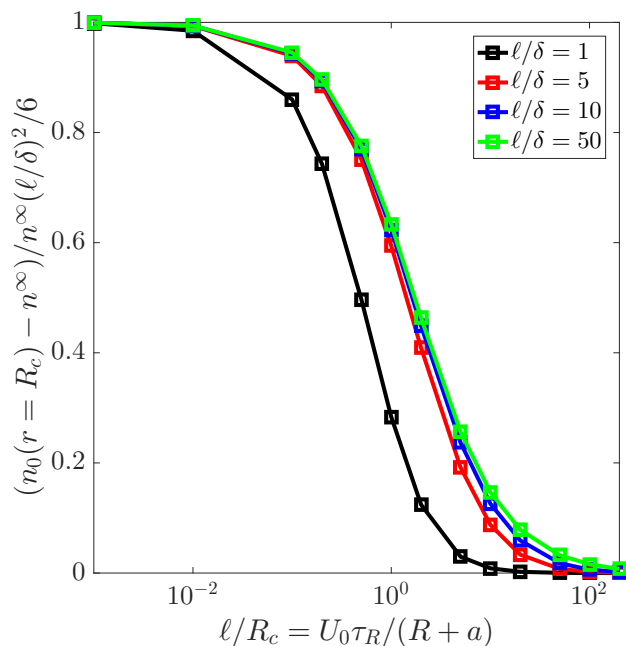


Fig. 3 Number density at the surface of a stationary, spherical probe $n_0(r = R_c)$, where $R_c = R + a$ is the sum of the probe size R and swimmer size a , minus the far-field number density n^∞ . This is scaled by $n^\infty (\ell/\delta)^2 / 6$, where $\ell = U_0 \tau_R$ is the run length of a swimmer, its speed U_0 times its reorientation time τ_R , and $\delta = \sqrt{D^{rel} \tau_R}$. The relative thermal diffusivity of a swimmer-probe pair is D^{rel} . We plot this quantity as a function of ℓ/R_c for a range of ℓ/δ . Note that the accumulation of swimmers is still large when $\ell \gg R_c$: $n_0 - n^\infty \sim n^\infty \ell R_c / \delta^2$. It is small on the scale of $(\ell/\delta)^2$.

sity of swimmers.) Even though this linear force-velocity relation is only guaranteed near equilibrium, we use the same definition for suspensions far from thermodynamic equilibrium²⁷. Thus, the effective drag $\langle \zeta \rangle$ (and mobility $\langle \mu \rangle$) and intrinsic microviscosity η^{micro} may now be functions of the external force or probe velocity: e.g. $\langle \mathbf{U}^{probe} \rangle \sim \mathbf{F}^{ext} \langle \mu(\mathbf{F}^{ext}) \rangle$.

From the detailed solutions to the PDEs derived above, we can directly compute the intrinsic microviscosity:

$$\eta^{micro} = \frac{3}{4\pi} \int_{r=R_c} (\hat{\mathbf{u}} \cdot \mathbf{n}) n'(\mathbf{r}; t) dS, \quad (15)$$

where dS has been scaled by R_c^2 . The intrinsic microviscosity will be determined solely by the microstructure at contact because we have neglected any long-ranged hydrodynamic or interparticle interactions in this paper. We calculate the full number density, polar order, and nematic order using a finite difference scheme adapted from Khair & Brady²¹ and implemented in MATLAB. We also compute the number density when $Pe \gg 1$ with a boundary-layer analysis (see Appendix A).

3 Stationary ($Pe \equiv 0$) and slow-moving ($Pe \ll 1$) probe

We briefly review the results from the stationary²⁶ and slowly-moving⁴ probe problems here. In the absence of probe motion, the suspension microstructure is isotropic. Activity of

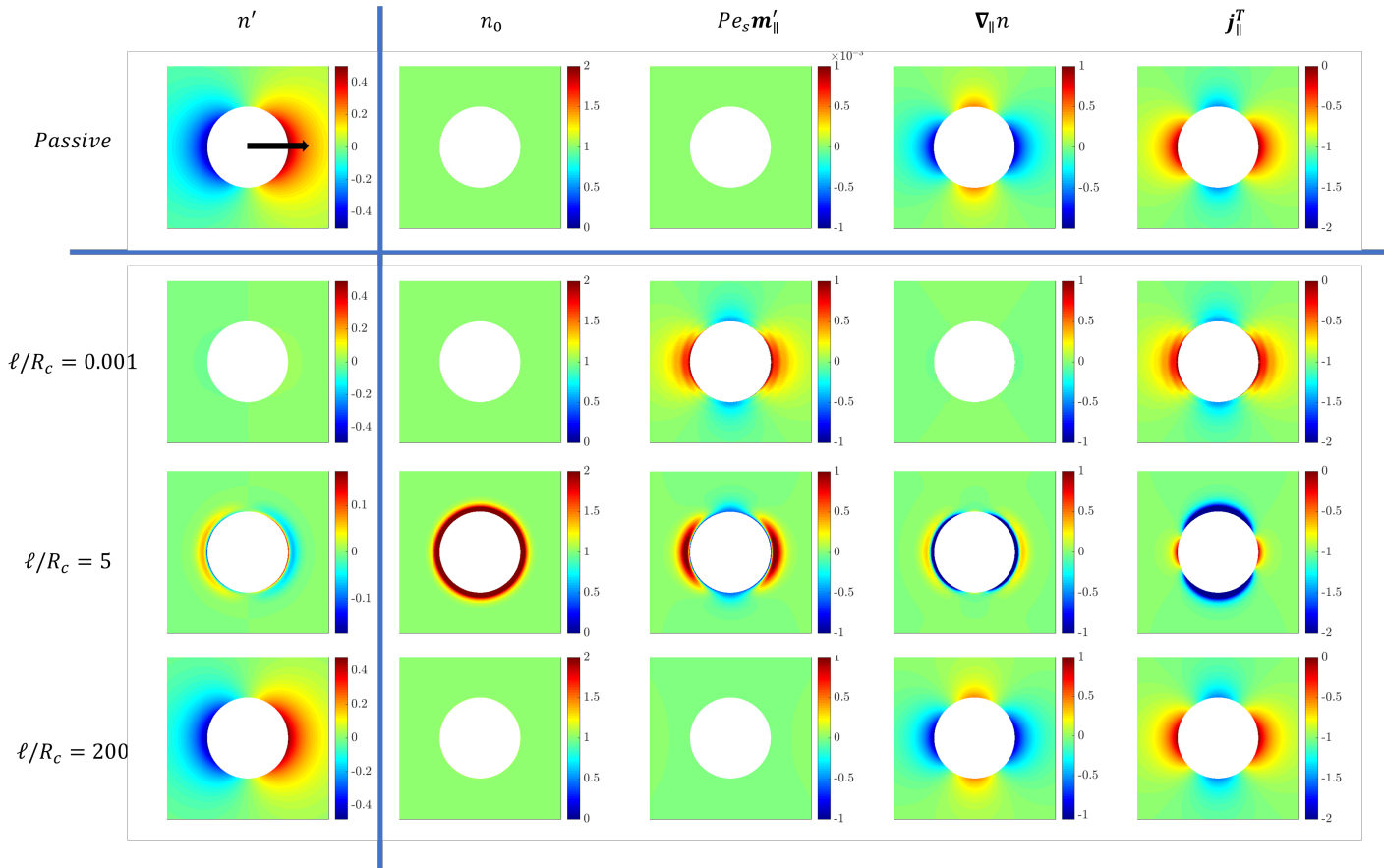


Fig. 4 Contour plots of the 3-D (axisymmetric) microstructure for weak external forcing $Pe = 0.001$; the direction of the external force is indicated with a solid black arrow. The background green colors indicates a uniform microstructure: $n', \mathbf{m}' \sim 0, n_0 = 1$. Red (warm) colors indicate an accumulation of particles, and blues (cold colors) indicate a depletion. For the active microstructures, $\ell/\delta = 10$. For the polar order $\mathbf{m}'_{||}$, concentration gradient $\nabla_{||} n'$, and flux $\mathbf{j}'_{||}^T$, the color indicates how strongly the field is aligned with (reds) or against (blues) the external force.

the swimmers is balanced by thermal diffusion, resulting in a swim-diffusive boundary layer at the probe surface of thickness $\delta/\sqrt{2((\ell/\delta)^2/6+1)}$. In Fig. 3 we plot this number density n_0 (the subscript 0 indicates a stationary probe) at the probe surface ($r = R_c$) as a function of ℓ/R_c , the ratio of the swimmers' run length to the characteristic length of excluded-volume interactions. A plot of the spatial variations of this number density may be found in the second-from-left column of Fig. 4.

The limit $\ell/R_c \ll 1$ is known as the “continuum limit.” In this regime, the run length of the swimmers is small compared to the probe size and the number density at the probe surface is given by $n_0 = n^\infty(1 + 1/6(\ell/\delta)^2)$. When $\ell/R_c \ll 1$, swimming is strong and most of the microstructural detail is confined to an $O(\delta/\sqrt{2((\ell/\delta)^2/6+1)})$ thin boundary-layer at the probe's surface (hence why it is invisible to the naked eye in the contour plots of n_0 and $\nabla n'$ in Fig.4). This boundary layer reflects a balance between swimming and thermal diffusion. As ℓ/R_c increases, the surface value of n_0 monotonically decreases; if one neglects nematic order, $\mathbf{Q} = \mathbf{0}$, this decrease goes as $(1 + \ell/\sqrt{3}R_c)^{-1}$. The physical reason for this decreased number density is that the swimmers no longer “see” the probe when $\ell \gg R_c$. When $\ell \ll R_c$, the swimmers collide with the probe and quickly reorient and move away, just like a Brownian particle. In contrast, when

$\ell \gg R_c$, the swimmers collide with the probe and slide along the surface until they are able to continue swimming freely; they reorient somewhere out in the bulk. Thus, the larger ℓ is compared to R_c , the farther away from the probe they are upon re-orientation, and the less likely they are to collide with the probe. As a result, the number density is reduced by a factor of ℓ/R_c : $n_0 \sim \ell R_c/\delta^2$. This number density may still be large, but is small on the scale of $(\ell/\delta)^2$.

In Figs. 5 and 6 we plot the intrinsic microviscosity as a function of ℓ/R_c for various values of the activity level ℓ/δ . We see that the qualitative trend of η^{micro} with respect to ℓ/R_c is consistent across values of ℓ/δ —when $\ell/R_c \ll 1$ or $\ell/R_c \gg 1$, $\eta^{micro} = 1$ as in a suspension of passive Brownian particles, and there is a minimum at $\ell \sim R_c$ that is dependent on the activity level. (The overshoot seen at $\ell/\delta = 50$ is a result of the choice of closure; finite element calculations in $2D^4$ reveal that the approach is monotonic.) We note that there is nearly exact agreement between the results in $d = 2$ and $d = 3$, as one would expect, and as is the case in passive suspensions.

To understand these results it helps to recall the behavior in a passive suspension. In a passive suspension the motion of the probe results in a small accumulation of bath particles in front of the probe and a small wake of equal magnitude behind the probe.

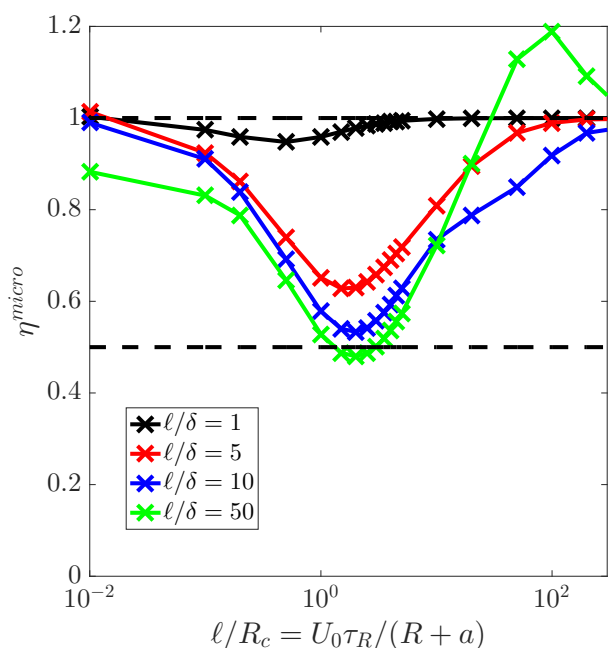


Fig. 5 Intrinsic microviscosity η^{micro} in $d = 3$ plotted as a function of $\ell/R_c \equiv U_0 \tau_R / (R + a)$, where U_0 is the speed of the swimmers, and τ_R is their reorientation time. Different colors indicate different levels of activity: $\ell/\delta = U_0 \tau_R / \sqrt{D^{rel} \tau_R}$, where D^{rel} is the relative thermal diffusivity. The dashed line at 1 is the microviscosity of a passive suspension at $Pe \ll 1$, and the dashed line at 0.5 is the microviscosity of a passive suspension as $Pe \rightarrow \infty$.

Because these particles are thermal, this concentration gradient results in a thermal force that pushes against the probe in front, and “sucks” it from behind (in the words of Squires & Brady²⁷)—this retards the motion of the probe (see the top row of Fig. 4). In the continuum limit, $\ell/R_c \ll 1$ (second row from the top of Fig. 4), the swimmers are effectively Brownian particles diffusing through the fluid with an active self-diffusivity $D_T(1 + 1/6(\ell/\delta)^2)$. Due to the accumulation boundary layer at the probe surface, the advective flux of swimmers is substantially larger than in a passive suspension $n_0 \mathbf{U}^{probe} \sim n^\infty(1 + 1/6(\ell/\delta)^2) \mathbf{U}^{probe}$. However, the effective diffusivity of the suspension is also increased, so there is a corresponding “thermal” flux of the same magnitude that counteracts this: $-D^{rel}(1 + 1/6(\ell/\delta)^2) \nabla n'$. The net reactive force on the probe is thus the same as found in a passive suspension $\eta^{micro} = 1$.

Curiously, $\eta^{micro} = 1$ when the active motion of the bath particles is decidedly non-Brownian on the length scale of the probe, $\ell/R_c \gg 1$ (see the right-hand side of Fig. 5). Physically, when a swimmer collides with the probe, it slides along the contact surface—this is enforced by the no-flux boundary condition—until it is able to swim away or reorient. Because $\ell \gg R_c$, the swimmer reorients infrequently, and thus slides along the surface until it is able to continue along its trajectory with the same orientation. The particles accumulate the surface of the probe as $n_0 \sim n^\infty \ell R_c / \delta^2$ (Fig. 4, bottom row, second column from the left). In this limit, the effective diffusivity of the suspension is balancing this advective disturbance scales as $D^{rel}(\ell R_c / \delta)^2$. Thus, the microviscosity is the same as found in passive suspensions.

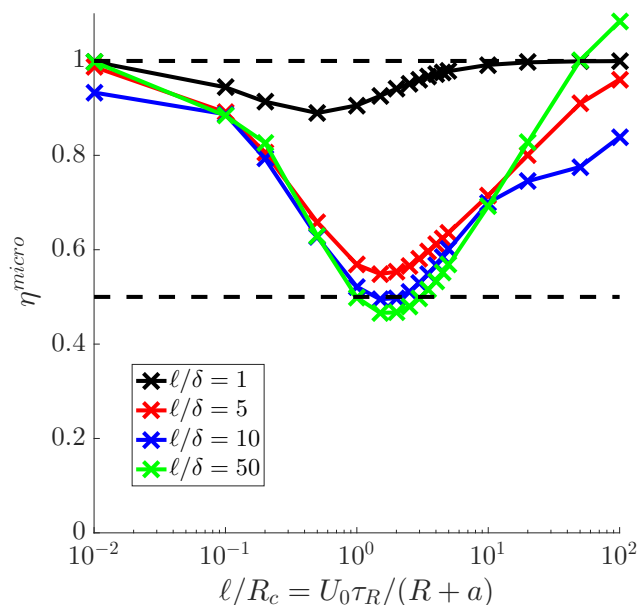


Fig. 6 Intrinsic microviscosity η^{micro} in $d = 2$ plotted as a function of $\ell/R_c \equiv U_0 \tau_R / (R + a)$, where U_0 is the speed of the swimmers, and τ_R is their reorientation time. Different colors indicate different levels of activity: $\ell/\delta = U_0 \tau_R / \sqrt{D^{rel} \tau_R}$, where D^{rel} is the relative thermal diffusivity. The dashed line at 1 is the microviscosity of a passive suspension at $Pe \ll 1$, and the dashed line at 0.5 is the microviscosity of a passive suspension as $Pe \rightarrow \infty$.

Experimentally, this indicates that both the microviscosity of a suspension of “smooth” swimming bacteria (i.e. bacteria that do not tumble) should be indistinguishable from a suspension of inactive bacteria. The linear microrheology problem cannot differentiate between the two; any difference would therefore be due to the hydrodynamic flow generated by the motile bacteria.

The nonmonotonic dependence of η^{micro} on ℓ/R_c is somewhat surprising initially, but this too has a simple physical interpretation. When $\ell \sim R_c$, a swimmer collides with the probe and slides along the surface as it does when $\ell/R_c \gg 1$, but it may still be near the probe when it reorients. For example, a swimmer approaching the front of the probe may collide and then slide around to the back of the probe. Once there, it can either reorient and swim away from the probe, or it can collide with the probe again and push it along—the latter scenario would result in a microviscosity less than one would find in a passive suspension. The opposite would be true of a particle approaching the rear of the swimmer—it could swim away in front or reorient and hit the probe, thereby increasing the microviscosity. Because the probe is in motion but the active process is isotropic, the swimmers are slightly more likely to push on the probe from behind than push against it out front. The microviscosity is thus reduced for $\ell/R_c \sim O(1)$; $\eta^{micro} \sim 1/2$ for highly active suspensions.

This is corroborated by the nested boundary-layer structure in the third row of Fig. 4. Because the rotational and translational motion are coupled through the polar (and nematic) order, there are two distinct boundary-layers that arise from activity: one that

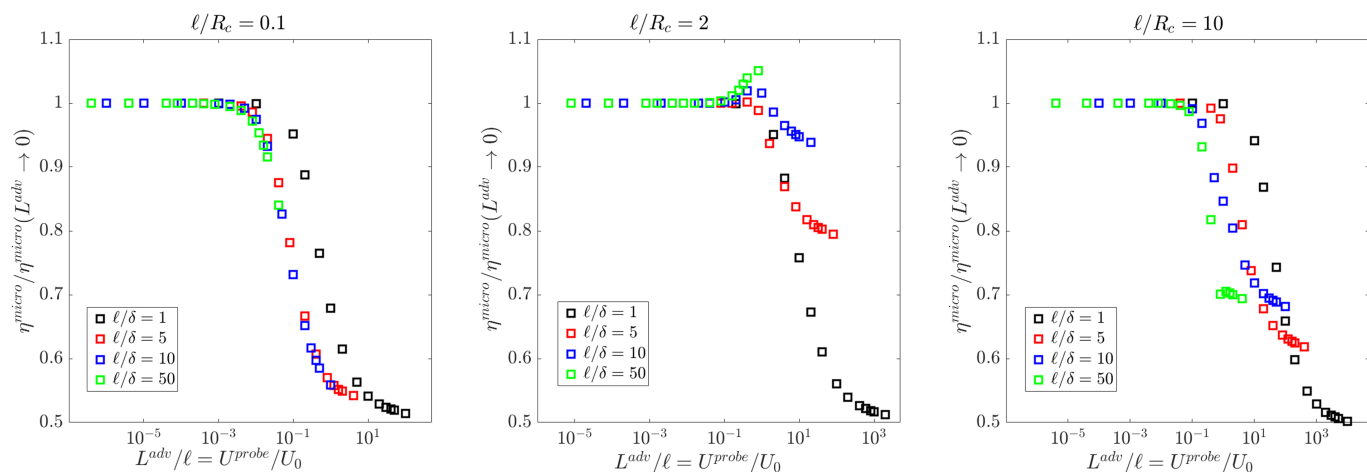


Fig. 7 Nonlinear intrinsic microviscosity ($d = 3$) η^{micro} plotted as a function of U^{probe}/U_0 for various $\ell/R_c = U_0 \tau_R / (R + a)$. The probe's speed is U^{probe} , R is the probe size, a is the swimmer size, U_0 is the speed of the swimmers, and τ_R is their reorientation time. Different colors indicate different levels of activity: $\ell/\delta = \sqrt{U_0^2 \tau_R / D^{\text{rel}}}$, where D^{rel} is the relative thermal diffusivity of a probe-swimmer pair.

is a distance $\delta/\sqrt{2(1/6(\ell/\delta)^2 + 1)}$ away from the probe surface (in 3-D), and another that is a distance δ from the probe surface, where $\delta = \sqrt{D^{\text{rel}} \tau_R}$ and $\ell = U_0 \tau_R$. The number density n' is screened by $\delta/\sqrt{2(1/6(\ell/\delta)^2 + 1)}$, and the polar order m' is screened by both $\delta/\sqrt{2(1/6(\ell/\delta)^2 + 1)}$ and $1/\delta$,³⁴ which is noticeable when $\ell \sim R_c$. The concentration disturbance n' is non-monotonic with distance from the probe surface. Closest to the probe $r - R_c \sim O(\sqrt{2(1/6(\ell/\delta)^2 + 1)})/\delta$, there is an accumulation of swimmers in front and a depletion in back; these swimmers are swimming against the probe. Just outside this boundary-layer, $r - R_c \sim O(1/\delta)$, there is instead an accumulation of swimmers behind the probe and a depletion out front. The swimmers in this outer boundary layer are swimming with the probe. Consider a swimmer that collides with the front of the probe (in the inner boundary layer). This swimmer opposes the motion of the probe, but slides along the surface until it is able to reorient. Because $\ell \sim R_c$, it is still close to the probe—in the outer boundary layer. It reorients and swims with the probe, again colliding with it and sliding along the surface but ending up in the inner boundary layer, again swimming against the probe. There is still a net drag on the probe, but because some of the swimmers in the probe's wake are reorienting and swimming around the probe again, the average concentration gradient decreases, and thus the intrinsic microviscosity decreases.

Interestingly, though the polar order (and thus the gradient in number density) are non-monotonic in r , the flux of swimmers relative to the probe is monotonic (third row of Fig. 4), and exhibits precisely the same qualitative behavior as in the absence of activity. Overall, Brownian motion is still trying to compensate for the wake left by the advective motion, and the swimmers assist Brownian motion because they are attracted to the probe surface.

Our findings are in qualitative agreement with the simulations of Reichhardt & Reichhardt²⁴ which compute a *decreased* mobility in an active bath without hydrodynamic interactions. Curiously, the authors find that the mobility monotonically decreases with ℓ/R_c at fixed $(\ell/\delta)^2/(\ell/R_c) = U_0 R_c / D^{\text{rel}}$ (the strength of activity

relative to thermal diffusion is fixed)²⁴, while our calculations indicate that the mobility should reach a maximum as $\ell/R_c \rightarrow \infty$ at fixed $(\ell/\delta)^2/(\ell/R_c)$. The simulations are primarily focused on studying tracer mobility as a way to probe the phase behavior of active matter; their most dilute calculations are at an area fraction of 18.85%. In this regime, the suspension is concentrated enough that the active run-and-tumble of the swimmers is hindered by steric interactions between swimmers themselves^{35,36}.

Both in the simulations²⁴ and our findings, the microviscosity is always greater than the viscosity of the embedding solvent $\langle \eta \rangle > \eta_s$. These findings stand in contrast to many theoretical predictions and measurements of reduced shear viscosity in bacterial suspensions^{12,37,38} and reduced microviscosity in an active nematic^{23,25}, which would require a negative intrinsic microviscosity; from a structural perspective, this would require us to have particles accumulate behind the probe and deplete in front of it. This indicates that hydrodynamic interactions may play an important qualitative role in the microrheology problem, either in the context of the swimmers' fluid velocity disturbance, or the interaction between the active random walk and the fluid velocity disturbance created by the probe.

4 Swiftly moving probe ($Pe \gtrsim 1$)

In a passive colloidal suspension the balance between advection and diffusion is confined to a boundary layer of thickness $R_c Pe^{-1}$ at the probe surface when $Pe \gtrsim O(1)$. The number density of bath particles in the boundary layer in front of the probe scales as Pe , ensuring that η^{micro} remains order one, even as the number of particles in the probe's path becomes orders of magnitude larger than the bulk number density. In the wake behind the probe, however, the concentration of particles cannot decrease below zero. Thus, the probe is no longer being sucked from behind by the thermal restoring force, it is only being slowed by the accumulation of particles in front. Hence, the suspension force-thins (analogous to shear-thinning; see top row of Fig. 8), and approaches $\eta^{\text{micro}} = 1/2$ as $Pe \rightarrow \infty$ (for both $d = 2$ and $d = 3$).

We previously found that activity lowers the intrinsic microviscosity in the linear-response regime, and indeed η^{micro} asymptotes to a value slightly less than $1/2$ as $\ell/\delta \rightarrow \infty$ for $\ell/R_c \sim O(1)$ when $Pe \ll 1^4$. The low-shear plateau is always lower than that found in a passive suspension ($\eta^{micro} = 1$), and indeed might even be lower than the large Pe plateau found in passive suspensions ($\eta^{micro} = 1/2$). When $Pe \rightarrow \infty$ and $\ell/\delta, \ell/R_c$ are finite, we expect to recover the passive suspension high- Pe plateau because the swimming will be obscured by advection. This indicates there must be a region where a highly active suspension is force-thickening even in the absence of any interparticle hydrodynamic interactions (HI), contact frictional forces, or fluid disturbances arising from self-propulsion.

When solving the microrheology problem for small Pe and arbitrary ℓ/δ and ℓ/R_c , we implicitly assumed that the distance moved by the probe during a time τ_R was less than the characteristic distance moved by the swimmers $L^{adv} = U^{probe} \tau_R \ll \ell$. Indeed, in Fig. 7, we see that the non-Newtonian microrheology is dictated by the ratio L^{adv}/ℓ —whether or not the swimmers can outrun the probe between reorientations.* The results for $L^{adv} \ll \ell$ are given in the previous section, and it is clear from Fig. 7 that $\eta^{micro} \rightarrow \eta^{micro}(Pe \rightarrow 0)$ in this limit. Correspondingly, in Fig. 8 we see that the advective disturbance to the microstructure is almost imperceptible for $\ell/R_c \lesssim O(1)$ and $Pe \gtrsim O(1)$ (i.e. $L^{adv} \lesssim O(1)$) because the bath particles can keep up with the probe.

When $Pe \gg 1$ swimmers accumulate in the advective-diffusive boundary layer at the probe surface (see the right-hand column of Fig. 8), and when $L^{adv} \gg \ell$, the swimmers cannot move farther than the probe does in a time τ_R . Thus, a swimmer behind the probe is unable to swim or diffuse into the probe's wake and has no chance of pushing the probe along from behind. Simultaneously, a swimmer in the boundary layer at the probe front surface cannot escape—it will remain in the probe's path even if it swims out of the advective-diffusive layer. As a result, the microviscosity (and as seen in the right-hand column of Fig. 8, the microstructure) is the same as found in passive suspensions at large Pe , $\eta^{micro} = 1/2$. In Fig. 7, this means that $\eta^{micro}/\eta^{micro}(Pe \rightarrow 0)$ will approach some value between ~ 1 and $1/2$ as $U^{probe}/U_0 \rightarrow \infty$, depending on ℓ/R_c and ℓ/δ .

The force-dependent microrheology (i.e. $L^{adv} \sim \ell$ depends on both ℓ/R_c and L^{adv}/ℓ ; the physical behavior is illustrated in Fig. 1. First consider the continuum limit, $\ell \ll R_c$ (leftmost panel of Fig. 7, top-left panel of Fig. 1, top row of Fig. 9). Because the run length is small compared to R_c , a swimmer in the probe's path will always be swept up into the advective-diffusive boundary layer—it can't swim out of the way between random reorientations regardless of the magnitude of L^{adv} . The microrheology in the continuum limit is thus always dictated by the balance between advection and diffusion. As we discussed in Section 3, the larger advective particle flux due to the increased concentration of swimmers at the probe surface is balanced by a diffusive flux of the same magnitude, because the swimmers appear to be “hot”

Brownian particles. When the probe starts to move more quickly, the advective-diffusive boundary layer becomes thinner, but the concentration of particles in that boundary layer increases with Pe in front of the probe. Behind the the probe, the concentration decreases but cannot decrease below zero. Indeed, in Fig. 9, we see only minor changes to the shape of the wake when $L^{adv} \sim \ell \ll R_c$ (c.f. panels (a) and (b)).

In the opposite limit, $\ell \gg R_c$ (rightmost panel of Fig. 7, bottom panel of Fig. 1, bottom row of Fig. 9), swimmers are still “attracted” to the probe, but are so persistent that they will typically collide with the probe, slide along the surface, and then keep swimming in the same direction before reorienting. When the probe is moving more quickly, swimmers in front of the probe will collide with it sooner (it is moving toward them as they are moving toward it), collide, and continue swimming away, just as before. At the same time it becomes more difficult for swimmers behind the probe to actually reach it—they may be unable to collide with it, or reorient shortly after colliding with it from behind. Some of the swimmers that do collide from behind will help push the probe along, so we would expect a small reduction in the microviscosity. We see the structural underpinnings of this behavior in the bottom row of Fig. 9. When $U^{probe} = U_0$, one can actually see the swim-diffusive boundary layer detach from the rear of the probe as ℓ/R_c increases in (h). These are plots of the stationary probability distribution, so this detached layer persists and “hovers” behind the probe. This structure pinpoints the spot on the corresponding curve in Fig. 7 where force-thinning begins. The suspension will force-thin until $L^{adv} \gg \ell$, at which point the swimmers behind the probe are completely unable to keep up with it, and there is no chance that they are able to help push the probe along (panel (j) of Fig. 9).

When $\ell \sim R_c$ and the probe moves slowly, swimmers are able to remain near the probe after a collision and push on it again after reorienting (see Fig. 4). This same mechanism explains a non-monotonic enhancement to the probe's effective diffusivity³⁹. When the probe starts moving in a particular direction, swimmers that approach it from behind aren't as easily able to slide along the surface to the front and push against the probe upon reorienting. On the other hand, swimmers that collide with the front of the probe are easily able to slide along the surface to the back, reorient, and push the probe along. When the probe starts to move more quickly, this mechanism is further modified (Fig. 1, top-right panel). Consider a swimmer in front of the probe that slides along to the back during a time τ_R . If the probe were moving slowly, the swimmer would then reorient and push the probe along. When the advection length is comparable to the run length, however, a swimmer will get to the back of the probe, but the probe will keep moving and it will be harder for the swimmer to keep up and push the probe along (see panel (d) of Fig. 9). Swimmers that collide with the back of the probe and swim along to the front, however, will still be within striking distance of the probe and have no trouble pushing against it. Thus, when $\ell \sim R_c$, the suspension will actually force-thicken until the swimmers are unable to keep up with the probe altogether (Fig. 7, center panel). The results indicate that the degree of force-thickening increases with ℓ/δ . We expect that there is some maximum degree of force-

* If $Pe \gg 1$ but $\ell \ll \delta$, the ratio L^{adv}/ℓ is no longer important because activity is weak.

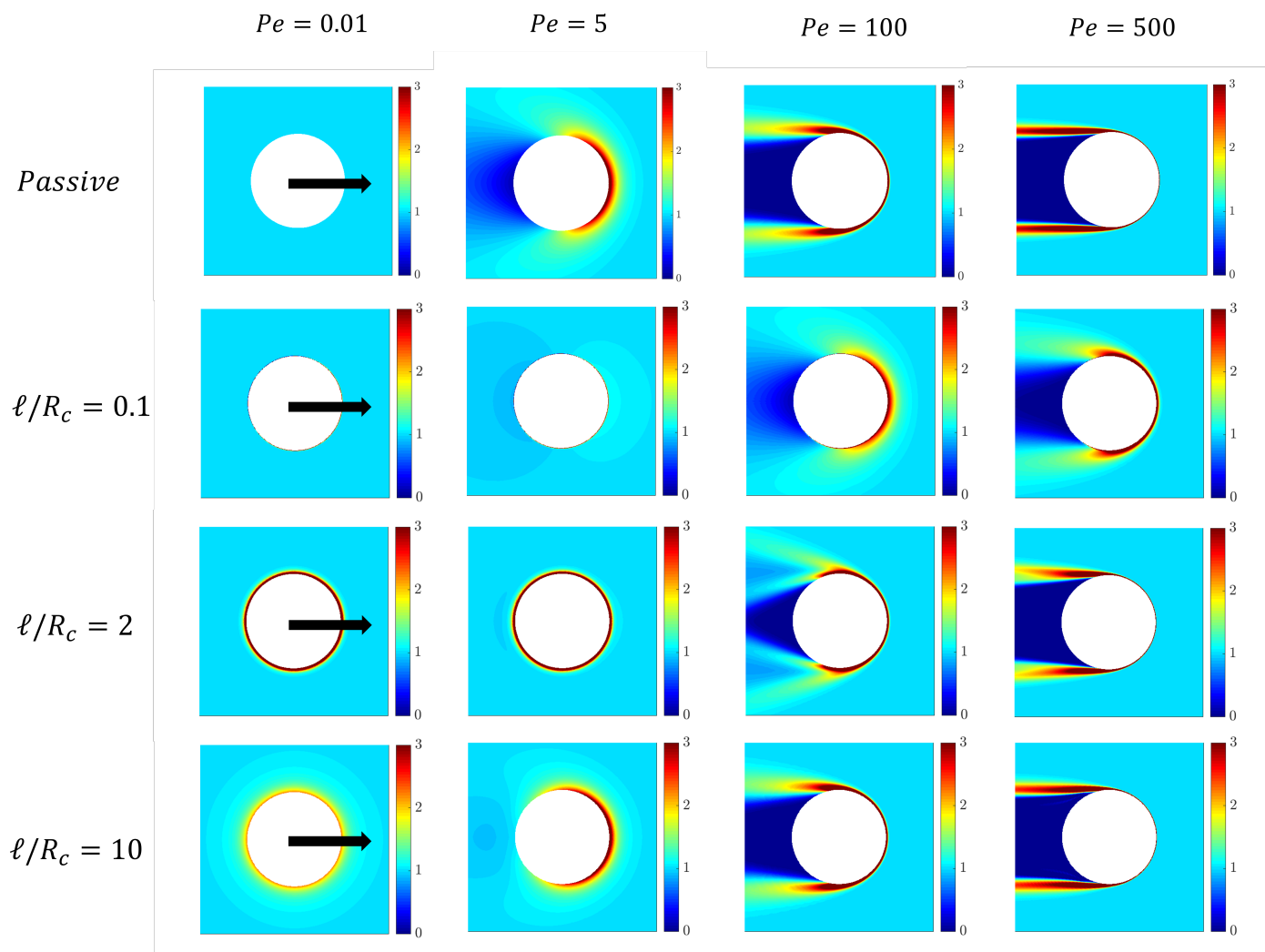


Fig. 8 Contour plots of the number density for various values of the external Péclet number $Pe = F^{ext}/(k_B T/a)$, where F^{ext} is the external force moving the probe (indicated by the black arrow) and a is the size of the bath particles, and the swim Péclet number $Pe_s = U_0 R_c/D^{rel}$ where U_0 is the swim speed, R_c is the center-to-center separation distance of a swimmer and the probe upon contact, and D^{rel} is the relative translational diffusivity of the pair. The activity level is fixed at $\ell/\delta = 10$.

thickening as $\ell/\delta \rightarrow \infty$, but are not numerically able to verify this. Note that, for $\ell/\delta = 50$ we do not show the approach to the final plateau due to numerical limitations. (For $Pe \sim O(10^4)$ we require a finer spatial resolution than possible with the desktop computer used.) This mechanism for force thickening is quite different than mechanisms arising from lubrication interactions or interparticle friction.

A curious feature of the suspension microstructure is a triangular wake behind the probe when $Pe = 100$ and $\ell \sim R_c$, as opposed to the more parabolic wake observed at larger Pe , and in passive suspensions^{27,29}. The formation of this triangular wake appears to occur at $L^{adv} \sim \ell$ (see panel (e) of Fig. 9), where advection and swimming are similar in magnitude, and the shape indicates that the swimmers are trying to fill in the advective void left behind the probe. Adjacent to this wake we also see symmetric “shocks” of concentration where the advective-diffusive boundary-layer separates from the probe and the swimmers are actually moving away from the wake.

The other panels of Fig. 9 reveal that the triangular wake and “shocks” of concentration arise only when the probe velocity slightly exceeds the bare swim speed—the swimmers are not quite able to keep up with the probe, but they still distort the shape of its wake by trying to swim into the depleted areas. In the last column of Figs. 8 and 9 the swimmers can no longer keep up with the probe, and we see the characteristic $O(Pe)$ long wake behind the probe, with the accumulation boundary-layer separating from the probe at the poles $\hat{u} \cdot \mathbf{n} = 0$. This shape is constant across the activity levels we depict in Figs. 8 and 9; however the accumulation boundary-layer “tails” are shorter when ℓ/R_c is smaller—c.f. right-hand column in Fig. 8. This is simply another physical manifestation of the activity trying to compensate for the advective disturbance—the swimmers want to swim with the probe so the advective wake is simply not as long.

In a typical experiment, the easiest quantity to manipulate is U^{probe} or L^{adv} , as the probe is typically controlled with magnetic tweezers. In suspensions of synthetic swimmers, one can also

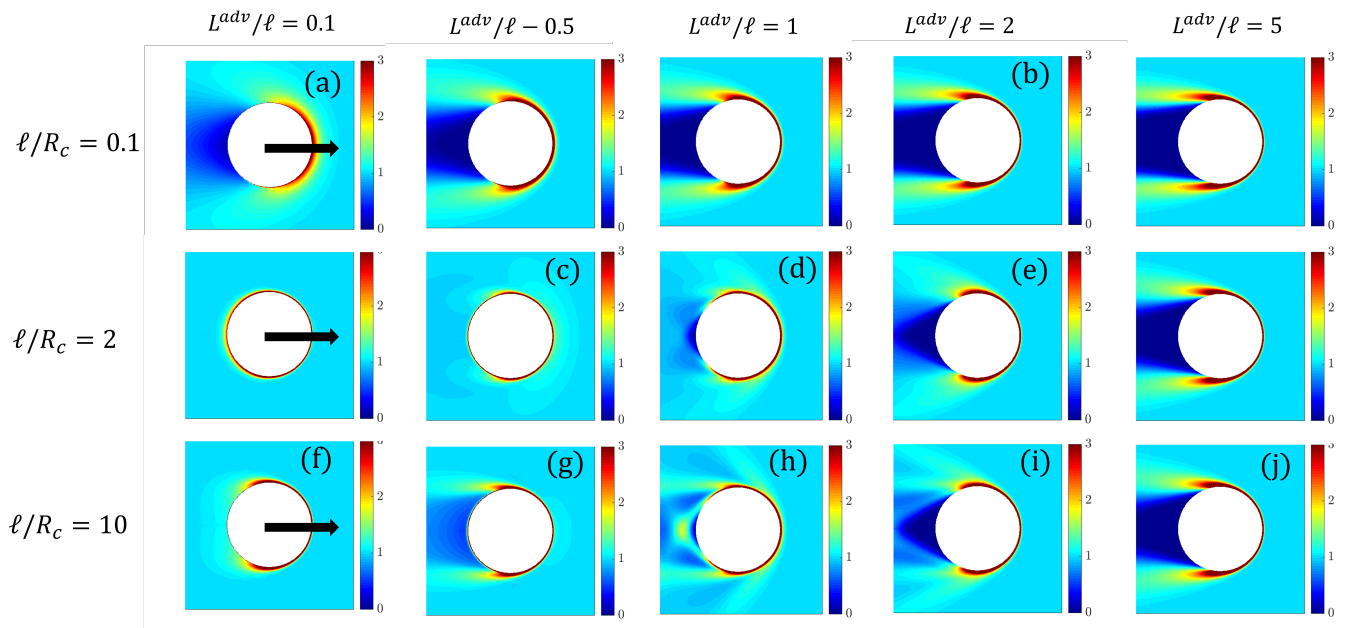


Fig. 9 Contour plots of the 3-D (axisymmetric) microstructure at $Pe = 100$ for various ratios of U_0/U^{probe} where U_0 is the swim speed of the bath particles and U^{probe} is the speed of the probe. The rows vary the value of ℓ/R_c . The background light blue color indicates a uniform microstructure: $n = n^\infty$, $\mathbf{m} = 0$. Red (warm) colors indicate an accumulation of particles, and darker blues (cold colors) indicate a depletion.

control U_0 or ℓ by altering the concentration of fuel. The probe size R and swimmer size a (and thus, the contact length R_c) as can also be controlled for synthetic particles, though τ_R is typically set by the swimmer size. Swimmer size, reorientation time, and swim speed are more difficult to control for self-propelled organisms. To check the predictions in Fig. 7, one could vary the probe size to change ℓ/R_c , and vary the probe speed to change L^{adv}/ℓ , both without having to control properties of the swimmers. One could repeat these experiments in suspensions of different organisms (e.g. smooth-swimming and tumbling *E. Coli*) to verify the dependence of η^{micro} on ℓ/δ .

It is noteworthy that the weak-force Newtonian plateau is much wider in active suspensions because the linear response regime is characterized by $L^{adv} \ll \ell$; the probe can actually move quite swiftly through an active suspension and remain in the linear response regime. The weak-force plateau is notoriously difficult to measure by either experiment or simulation; a wider plateau would allow one to make a linear response measurement at much higher probe speeds, where the average velocity (or force) is more readily distinguishable from Brownian fluctuations.

5 Conclusions

Using familiar frameworks from the study of passive colloidal suspensions, we investigated the nonlinear microrheology of a suspension of active Brownian particles (ABPs). We found that, in the absence of hydrodynamic interactions, the suspension swithins regardless of the hydrodynamic propulsion mechanism of the swimmer when $Pe = U^{probe} R_c / D^{rel} \ll 1$. We found that this low- Pe Newtonian plateau persists for a wide range of Péclet numbers, and that the width of the Newtonian plateau is set by the ratio of the swim speed to the probe speed (Fig. 7). The persistence of this plateau reflects the fact that the swimmers are able to fill

in the void created by the probe's advective motion when $L^{adv} < \ell$ and $\ell \gtrsim R_c$. If the run length is short compared to the distance the probe travels in τ_R , the swimmers will reorient before they are able to reach the probe even when $\ell \gtrsim L^{adv}$; in this limit the wake (and viscous response) resembles that of a passive suspension. When $\ell \ll L^{adv}$, the effects of activity vanish and we recover the familiar high Pe plateau from previous work on passive suspensions²⁷. Most of these effects are predictive; there are no experimental studies to-date that measure the microviscosity of an active suspension, though there is a computational study examining various phase behaviors in the microrheology problem²⁴. Reichhardt & Reichhardt compute the mobility of a probe in an active bath (neglecting hydrodynamic interactions and Brownian motion), and find *reduced* probe mobility, even at low volume fractions. This is consistent with our findings that the intrinsic microviscosity is positive in the absence of HI.

Hydrodynamic interactions in passive suspensions have been shown to cause quantitative changes in the non-equilibrium mechanical properties of a suspension, and more importantly produce qualitatively different behaviors. The most notable example of this is that near-field hydrodynamic interactions lead to force-thickening of the suspension at high shear rates^{16,21}. In active suspensions, hydrodynamic interactions have been shown to alter the particle-phase pressure⁴⁰ and shear viscosity^{12,37,38}, but these effects do not alter the problem's boundary-layer structure⁴⁰. The same balances between advection, diffusion, and activity seen here are expected to hold, but the parameters D^{rel} , τ_R , and F^{ext} or U^{probe} will now depend on the strength of hydrodynamic interactions through familiar mobility formalisms in low Reynolds number fluid-mechanics⁴¹. Incorporation of the hydrodynamics does not require us to say anything about the propulsive mechanism of the bath particles, though the framework presented

in previous works is readily modified to include specifications of the swimmers' gait. We will discuss the role of HI in a future study.

A Boundary-layer analysis, $Pe \gg 1$

When advection is strong $Pe \gg 1$, there will be a thin boundary layer of $O(Pe^{-1})$ at the surface of the probe over which diffusion balances advection. For simplicity, we assume that, outside the advective-diffusive boundary layer, the microstructure is uniform $n = 1$ and $\mathbf{m} = 0$ – the effects of activity are contained within the advective-diffusive layer. We choose a boundary-layer coordinate $Y = Pe(r - 1)$, thus amplifying all of the gradients in the governing equations by Pe . We then expand the concentration and polar order in powers of Pe^{-1} : $n = Pen_0 + n_1 + O(Pe^{-1})$, $\mathbf{m} = Pem_0 + m_1 + O(Pe^{-1})$. Due to the advective build-up of bath particles near the surface, the leading order terms must scale with the Péclet number.

In the boundary layer, the governing equations reduce to

$$\frac{\partial n_0}{\partial Y} + \mu n_0 = \frac{\ell}{L^{adv}} m_{r,0}, \quad (16)$$

$$\frac{\partial^2 m_{r,0}}{\partial Y^2} + \mu \frac{\partial m_{r,0}}{\partial Y} - 2 \frac{\delta^2}{L^{adv2}} m_{r,0} = \frac{1}{3} \frac{\ell}{L^{adv}} \frac{\partial n_0}{\partial Y}, \quad (17)$$

$$\frac{\partial m_{r,0}}{\partial Y} + \mu m_{r,0} = \frac{1}{3} \frac{\ell}{L^{adv}} n_0, Y = 0, \quad (18)$$

$$m_{r,0} \sim 0, Y \rightarrow \infty, \quad (19)$$

$$\frac{\partial^2 m_{\mu,0}}{\partial Y^2} + \mu \frac{\partial m_{\mu,0}}{\partial Y} - 2 \frac{\delta^2}{L^{adv2}} m_{\mu,0} = 0, \quad (20)$$

$$\frac{\partial m_{\mu,0}}{\partial Y} + \mu m_{\mu,0} = 0, Y = 0, \quad (21)$$

$$m_{\mu,0} \sim 0, Y \rightarrow \infty, \quad (22)$$

where $\mu \equiv \mathbf{u} \cdot \mathbf{n}$ and m_r and m_μ are the radial and angular components of the polar order. We neglect nematic order in this calculation as it is unimportant when advection dominates. Because $m_{\mu,0}$ is de-coupled from n_0 and $m_{r,0}$, we may assume that it is unimportant at $O(Pe)$ and derive a third-order equation for n_0 :

$$\frac{\partial^3 n_0}{\partial Y^3} + 2\mu \frac{\partial^2 n_0}{\partial Y^2} + \mu^2 \frac{\partial n_0}{\partial Y} - \lambda^2 \frac{\partial n_0}{\partial Y} - 2 \frac{\delta^2}{L^{adv2}} \mu n_0 = 0,$$

$$\frac{\partial^2 n_0}{\partial Y^2} + 2\mu \frac{\partial n_0}{\partial Y} + \mu^2 n_0 = \frac{1}{3} \left(\frac{\ell}{L^{adv}} \right)^2 n_0, Y = 0, \quad (23)$$

$$n_0 \sim 0, \quad \frac{\partial n_0}{\partial Y} + \mu n_0 \sim 0, Y \rightarrow \infty,$$

which has exponential solutions $f(\mu, L^{adv}/\ell, \delta/L^{adv}) e^{g(\mu, L^{adv}/\ell, \delta/L^{adv})Y}$. Note that we have defined $\lambda = \sqrt{1/3(\ell/L^{adv})^2 + 2(\delta/L^{adv})^2}$ for brevity. The function g is given by solutions to the characteristic equation

$$g(g + \mu)^2 = \left(\frac{\delta}{L^{adv}} \right)^2 + g\lambda^2. \quad (24)$$

This equation will have three roots, one of which leads to an unphysical exponential growth. The other two roots are exponentially screened oscillating functions of $\lambda, \delta/L^{adv}$ and μ .

We neglect terms of $O(\delta/L^{adv})$ to reduce the order of the characteristic equation (using the no-flux boundary condition). In doing this we assume that the distance moved by the probe in τ_R is much greater than distance the pair moves by Brownian motion in the same time, which is reasonable for a fast-moving probe that is similar in size to or much larger than the swimmers.

We can solve the reduced characteristic equation for n_0 :

$$n_0 = A(\mu) e^{-Y(\mu+\lambda)} + B(\mu) e^{-Y(\mu-\lambda)}. \quad (25)$$

This gives the correct result in the limit $\lambda \rightarrow 0$ and decays as $e^{-(\ell/\delta)(r-1)}$ when activity dominates advection.

To find the functions $A(\mu)$ and $B(\mu)$, one must go to the next order in Pe^{-1} :

$$n_0 \sim 1 + \frac{Pe}{2} (\mu + \lambda) e^{-Pe(r-1)(\mu+\lambda)}, \quad (26)$$

when $\lambda > |\mu|$. When $\lambda < |\mu|$, the concentration of bath particles behind the probe ($\mu < 0$) is zero, in front of the probe ($\mu > 0$), we find that the accumulation of particles is:

$$n_0 = 1 + \frac{Pe}{4} (\mu + \lambda) e^{-Pe(r-1)(\mu+\lambda)} + \frac{Pe}{4} (\mu - \lambda) e^{-Pe(r-1)(\mu-\lambda)}. \quad (27)$$

This microviscosity is thus:

$$\eta^{micro} = \frac{1}{2} [1 + \lambda^3], \quad \lambda < 1 \quad (28)$$

$$\eta^{micro} = 1, \quad \lambda > 1. \quad (29)$$

The first result indicates that the suspension must force-thin when $Pe \gg 1$, but the thinning goes as λ^3 . Activity increases the concentration of bath particles inside the advective-diffusive boundary layer, increasing the total drag on the probe. The second indicates that, when external forcing is strong, but swimming stronger, the microviscosity is equal to 1—the linear-response value for $\ell/R_c \gg 1$. Even though the suspension is being strongly driven from equilibrium by an external force, the swimmers are fast enough to fill in the wake left by the probe, so the suspension remains Newtonian. When the external force increases, the swimmers can no longer keep up, and we approach the result for a passive suspension.²⁷

References

- 1 S. Ramaswamy, *Annu. Rev. Condens. Matter Phys.*, 2010, **1**, 323–345.
- 2 M. C. Marchetti, J. F. Joanny, S. Ramaswamy, T. B. Liverpool, J. Prost, M. Rao and R. A. Simha, *Rev. Mod. Phys.*, 2013, **85**, 1143–1189.
- 3 D. T. N. Chen, A. W. Lau, L. A. Hough, M. F. Islam, M. Goulian, T. C. Lubensky and A. G. Yodh, *Phys. Rev. Lett.*, 2007, **99**, 148302.
- 4 E. W. Burkholder and J. F. Brady, *J. Chem. Phys.*, 2019, **150**, 184901.

- 5 G. Subramanian and D. L. Koch, *J. Fluid Mech.*, 2009, **632**, 359.
- 6 D. L. Koch and G. Subramanian, *Annu. Rev. Fluid Mech.*, 2011, **43**, 637–659.
- 7 A. Sokolov and I. S. Aranson, *Phys. Rev. Lett.*, 2012, **109**, 248109.
- 8 A. Zöttl and H. Stark, *Phys. Rev. Lett.*, 2014, **112**, 118101.
- 9 F. Alarcón and I. Pagonabarraga, *J. Mol. Liq.*, 2013, **185**, 56–61.
- 10 D. Grossman, I. S. Aranson and E. Ben-Jacob, *New J. Phys.*, 2008, **10**, year.
- 11 J. M. Yeomans, *Riv. del Nuovo Cim.*, 2017, **40**, 1–31.
- 12 H. M. López, J. Gachelin, C. Douarche, H. Auradou and É. Clément, *Phys. Rev. Lett.*, 2015, **115**, 028301.
- 13 A. Loisy, J. Eggers and T. B. Liverpool, *Phys. Rev. Lett.*, 2018, **121**, 018001.
- 14 D. Saintillan, *Exp. Mech.*, 2010, **50**, 1275–1281.
- 15 H. Brenner, *J. Fluid Mech.*, 1962, **12**, 35–48.
- 16 J. Bergenholtz, J. F. Brady and M. Vacic, *J. Fluid Mech.*, 2002, **456**, 239–275.
- 17 N. J. Wagner and J. F. Brady, *Phys. Today*, 2009, **62**, 27–32.
- 18 T. M. Squires and T. G. Mason, *Annu. Rev. Fluid Mech.*, 2010, **42**, 413–438.
- 19 D. Wirtz, *Annu. Rev. Biophys.*, 2009, **38**, 301–326.
- 20 S. Ebbens, *Curr. Opin. Colloid Interface Sci.*, 2016, **21**, 14–23.
- 21 A. S. Khair and J. F. Brady, *J. Fluid Mech.*, 2006, **557**, 73.
- 22 N. J. Hoh, *PhD thesis*, California Institute of Technology, 2013.
- 23 G. Foffano, J. S. Lintuvuori, A. N. Morozov, K. Stratford, M. E. Cates and D. Marenduzzo, *Eur. Phys. J. E*, 2012, **35**, year.
- 24 C. Reichhardt and C. J. O. Reichhardt, *Phys. Rev. E - Stat. Nonlinear, Soft Matter Phys.*, 2015, **91**, 032313.
- 25 G. Foffano, J. S. Lintuvuori, K. Stratford, M. E. Cates and D. Marenduzzo, *Phys. Rev. Lett.*, 2012, **109**, 1–5.
- 26 W. Yan and J. F. Brady, *Soft Matter*, 2015, **11**, 6235–6244.
- 27 T. M. Squires and J. F. Brady, *Phys. Fluids*, 2005, **17**, 1–21.
- 28 D. Saintillan and M. J. Shelley, *Complex Fluids Biol. Syst.*, Springer, New York, 2015, ch. 9, pp. 319–355.
- 29 R. N. Zia and J. F. Brady, *J. Fluid Mech.*, 2010, **658**, 188–210.
- 30 N. J. Hoh and R. N. Zia, *Lab Chip*, 2016, **16**, 3114–3129.
- 31 D. Saintillan and M. J. Shelley, *Comptes Rendus Phys.*, 2013, **14**, 497–517.
- 32 J. W. Swan and R. N. Zia, *Phys. Fluids*, 2013, **25**, year.
- 33 J. F. Brady, *J. Chem. Phys.*, 1993, **98**, 3335.
- 34 W. Yan and J. F. Brady, *Soft Matter*, 2017, **14**, 279–290.
- 35 S. C. Takatori, W. Yan and J. F. Brady, *Phys. Rev. Lett.*, 2014, **113**, 028103.
- 36 S. C. Takatori and J. F. Brady, *Soft Matter*, 2015, **11**, 7920–7931.
- 37 A. Sokolov and I. S. Aranson, *Phys. Rev. Lett.*, 2009, 148101.
- 38 D. Saintillan, *Phys. Rev. E - Stat. Nonlinear, Soft Matter Phys.*, 2010, **81**, 056307.
- 39 E. W. Burkholder and J. F. Brady, *Phys. Rev. E - Stat. Nonlinear, Soft Matter Phys.*, 2017, 052605.
- 40 E. W. Burkholder and J. F. Brady, *Soft Matter*, 2018, **14**, 3581–3589.
- 41 S. Kim and S. J. Karilla, *Microhydrodynamics : Principles and Selected Applications*, Dover, 1991.